CHAPTER 8: CATHODES FOR POLARIZED ELECTRON BEAMS

MATTHEW POELKER

Thomas Jefferson National Accelerator Facility
M/S Bldg. 5A, Room 500-17
12050 Jefferson Ave.
Newport News, VA 23606

Keywords

Polarized Electrons, GaAs, Semiconductor, Superlattice, Strained Superlattice, Negative Electron Affinity, Vent-Bake Photogun, Load-Lock Photogun, Ion Bombardment, Cathode Degradation, Activation, Hydrogen Cleaning, Fiber Laser, Gain Switching, Spin Manipulation, Mott's Polarimeter

Abstract

Cathodes that can deliver spin polarized electrons with high quantum efficiency are unique and need special preparation and handling. In this chapter, we discuss the physics underpinning of GaAs as the source for polarized electrons and methods to increase the QE and the degree of polarization simultaneously. Since this cathode is very sensitive to contaminants, we also describe two methods of incorporating the cathode into the high voltage DC photogun. The back bombardment of ions on the cathode in this gun is the limiting factor for the life-time of such a cathode. We present strategies to mitigate this effect as well as step-by-step procedure for cathode preparation. Since the excitation of GaAs for spin polarized electrons is wavelength sensitive, we have devoted a section to this drive laser. We conclude with a brief section on polarimetry, spin manipulation and future directions of research that may benefit this field.

8.1 INTRODUCTION

Many accelerator-based nuclear- and particle-physics experiments require a spin-polarized electron beam [8.1], *viz* a beam wherein the spin axes of the electrons within each accelerated bunch are aligned in a preferential direction. Electron spin can be another "tool" in the physicist's tool bag; one that enhances studies of nuclear structure, the dynamics of strong interactions, electro-weak nuclear physics including parity-violation, physics beyond the Standard Model and more [8.2]. Electron beams at accelerator storage rings "self-polarize" *via* Sokolov-Ternov synchrotron spin-flip radiation; however, at other types of accelerators a direct source of polarized electrons is required.

The first polarized-electron source for an accelerator, based on the photo-ionization of state selected ^{6}Li atoms, was developed at Yale University in the early '70s for the Stanford Linear Accelerator Center (SLAC) [8.3]. In 1977, a polarized electron source based on the Fano effect in rubidium was constructed for the Bonn synchrotron [8.4]. Other polarized sources were developed or proposed during the '70s, including an improved version of the ^{6}Li photo-ionization source [8.5], a source based on the chemical ionization of metastable He atoms [8.6], and sources using the Fano effect in Cs [8.7]. Despite some technical demonstrations, none of these latter sources ever became operational in accelerators. After the 1974 demonstration of polarized photoemission from GaAs [8.8] at low voltage, researchers at SLAC constructed a high voltage source [8.9] to conduct the seminal parity violation experiment E122 [8.10] that verified Wienberg and Salam's predictions and thereby helped to establish the Standard Model of electro-weak physics. Since then, DC high voltage polarized electron sources based on GaAs photocathodes were built and have operated at several laboratories, including Nagoya University [8.11], the Mainz Microtron [8.12], [8.13], the MIT-Bates Laboratory [8.14], NIKHEF [8.15], Bonn University [8.16] and CEBAF/Jefferson Lab [8.17].

There are four basic requirements for constructing a DC high voltage spin-polarized electron source using GaAs photocathodes:

1. atomically clean GaAs photocathode material,
2. an appropriate high voltage cathode/anode accelerating structure free of field emission,
3. an ultra-high vacuum (UHV) chamber, and,
4. a suitable drive laser.

Paying proper attention to these requirements will enable researchers to build a good spin-polarized electron source, where ***good*** describes a source that delivers a highly polarized beam at the desired current for a long time.

I note that some of the topics above are described in other chapters, particularly Chapter 4 on DC photoinjectors and Chapter 9 on photoinjector drive lasers. To avoid redundancy, this chapter will focus on issues specifically related to generating spin-polarized electron beams.

8.2 GaAs: A SOURCE OF POLARIZED ELECTRONS

GaAs is a direct transition III-V semiconductor with zincblende crystal structure [8.18], [8.19]. It can absorb laser light across the broad visible spectrum, but only illumination with near-IR wavelengths provides polarized photoemission. This is understandable by looking at the energy level diagram of GaAs. Figure **8.1** shows detailed and simplified representations [8.20] of the band structure, as described in the figure caption. Electron spin-orbit coupling splits the $P_{1/2}$ and $P_{3/2}$ energy levels of the valence band into two states separated by 0.34 eV, *i.e.*, large enough to avoid optical excitation from the lower energy $P_{1/2}$ state. Polarized photoemission takes advantage of the quantum-mechanical selection rules, *viz*, for circularly polarized laser light, conservation of angular momentum requires that an electron's spin-angular momentum quantum number to change by one unit, $\Delta m_j = \pm 1$. Furthermore, some transitions are more favorable than others, as indicated by the transition probabilities in Figure **8.1(c)**. So, by using circularly polarized laser light with photon energy equal to near-band gap energy, the conduction band can be populated preferentially with a particular spin state.

Polarization is defined as

$$P = \frac{N\uparrow - N\downarrow}{N\uparrow + N\downarrow} \tag{8.1}$$

where N refers to the number of electrons in the conduction band of each spin state, "up" or "down". For bulk GaAs, the theoretical maximum polarization is 50%, corresponding to three electrons of the desired spin state and one electron with opposite spin. However, in practice, due to various depolarization mechanisms, such as the Bir-Aronov-Pikus process [8.21], the D'Yankonov-Perel process [8.22], the Elliot-Yafet process [8.23], [8.24], and radiation trapping [8.25], the maximum polarization from the bulk is typically 35%. A less detailed description simply attributes depolarization to imperfections within the photocathode material that reduce the diffusion length. This will prevent electrons from efficiently reaching the photocathode surface, as well as providing a greater probability for the electrons to depolarize.

The figure of merit of polarized-electron beam experiments is a measure of how quickly an experiment can be performed with a desired level of accuracy. The figure of merit scales with P^2I, where P refers to polarization and I refers to the beam current. Hence, there is a great incentive to increase the beam's

polarization, particularly for experiments that cannot accommodate a high current, for example due to concerns over the failure of the target window or over cryogenic target boiling. Significant breakthroughs in the development of polarized electron sources occurred in the '90s, when groups at SLAC and Nagoya University independently developed a means to eliminate the heavy-hole/light-hole degeneracy at the valence-band maxima by introducing an axial strain within the GaAs crystal [8.26]–[8.28]. This was accomplished by growing GaAs atop GaAsP to introduce a strain resulting from the lattice mismatch between the GaAs and GaAsP crystal structures. Such a structure delivers polarization as high as ~75%, however the photocathode yield, or quantum efficiency (QE), typically is very low, just 0.1% (QE is discussed below). The GaAs surface layer is usually 50-100 nm thick. Thicker layers can provide higher QE, but then the strain relaxes and polarization is reduced.

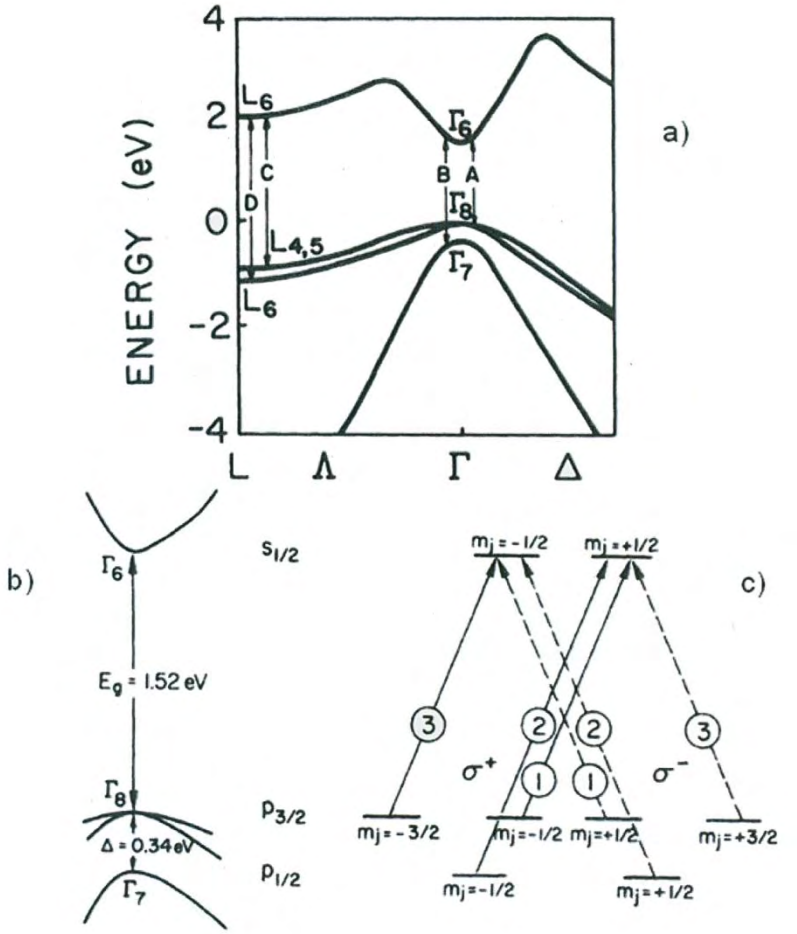

Figure 8.1. Energy level diagrams of GaAs: (a) Detailed band structure of GaAs; (b) "close-up" view near valance band maxima/conduction band minima; and, (c) simplified view showing individual spin-angular momentum states and transition probabilities, circled. [Reprinted figures with permission from [8.20]. Copyright 1976 by the American Physical Society]

Today's state of the art high polarization photocathode is the GaAs/GaAsP strained-superlattice structure [8.29], [8.30] consisting of a very thin GaAs surface layer (~5 nm) grown atop 10-20 pairs of thin, alternating layers of GaAsP and GaAs. These very thin GaAs layers maintain the strain, which improves polarization. Using many thin layers of GaAs/GaAsP raises the QE considerably higher than that obtained from a single (thicker) layer of strained GaAs since the electrons in sub-surface layers efficiently tunnel through the thin GaAsP layers. The net result is a polarization ~85% and a QE ~1%. Figure **8.2** represents each high polarization photocathode schematically with plots of polarization versus laser wavelength [8.31].

Both of the photocathode structures are commercially available [8.32], [8.33] thanks to collaborative R&D programs initiated by SLAC *via* the Department of Energy's (DOE) Small Business Innovative Research (SBIR) program. University groups in Japan and Russia have made similar photocathodes [8.34], [8.35] with different stoichiometric combinations of Ga, As and P, as well as In and Al to modify the band gap, and correspondingly the appropriate drive laser wavelength.

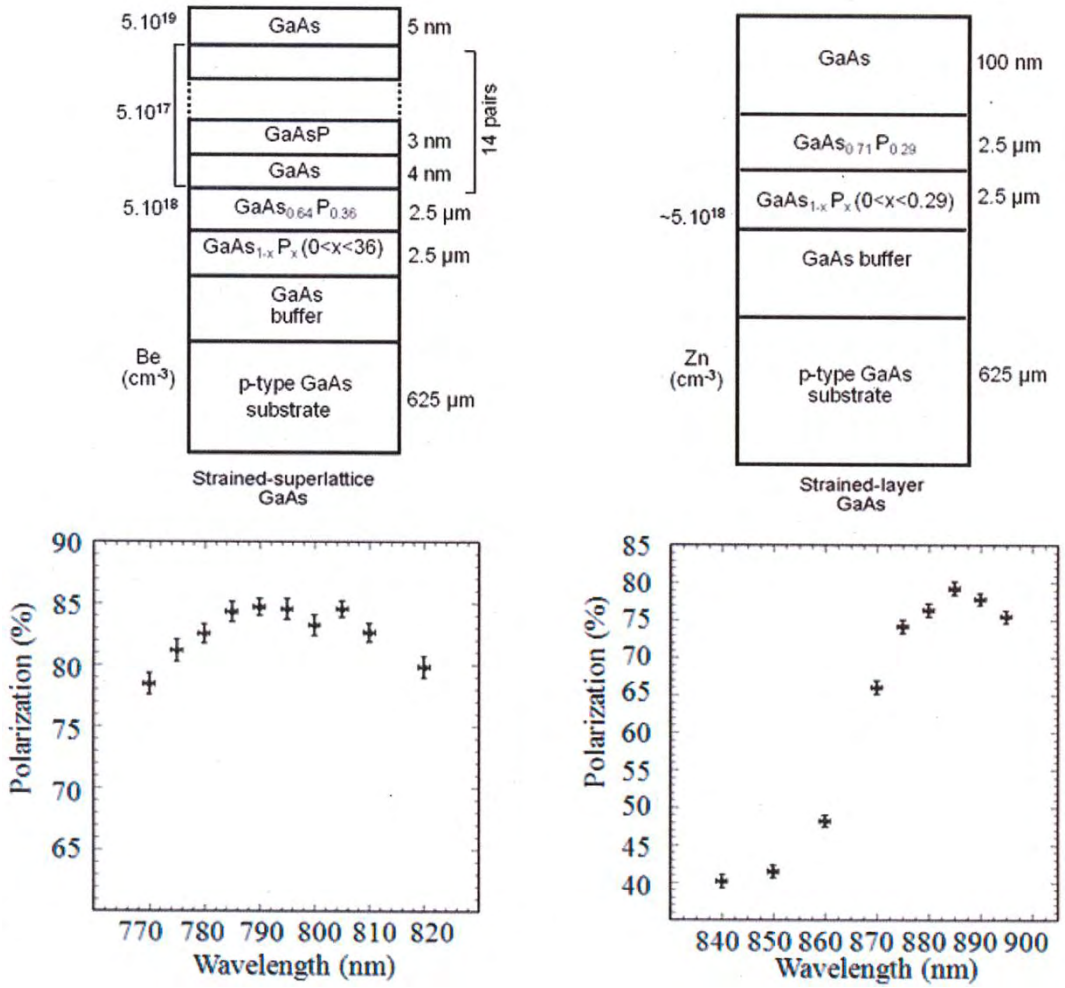

Figure 8.2. Two types of GaAs photocathode structures that provide high polarization: Spectral dependence of polarization for (left) strained-superlattice GaAs and (right) strained-layer GaAs. [Reprinted figure with permission from [8.31]. Copyright 2005 by the American Physical Society]

As detailed in Chapter 5, the emission of electrons from cathodes, such as GaAs, often is described by the three-step process [8.36] involving the absorption of light, the diffusion of electrons to the surface of the photocathode and the emission of the electrons into the gun vacuum chamber. GaAs is a strong absorber, absorbing most of the light within a few hundred nanometers. As described above, absorption of circularly polarized light with near-band gap energy preferentially populates the conduction band with spin-polarized electrons. These electrons diffuse in all directions and those that move toward the surface encounter a potential barrier known as the electron affinity (Figure **8.3(a)**). A requirement for efficient photoemission is that the GaAs is p-doped [8.8], which lowers the Fermi level throughout the material. The p-doping also lowers the conduction band at the surface of the photocathode, which, in turn decreases the electron affinity (Figure **8.3(b)**). Still, no significant photoemission is obtained until the potential barrier is reduced further; this is accomplished by adding a mono-layer of cesium and an oxidant to the photocathode (Figure **8.3(c)**), a

process called "activation". When the vacuum energy level is reduced below that of the conduction band of the intrinsic material, a negative electron affinity (NEA) condition is said to exist.

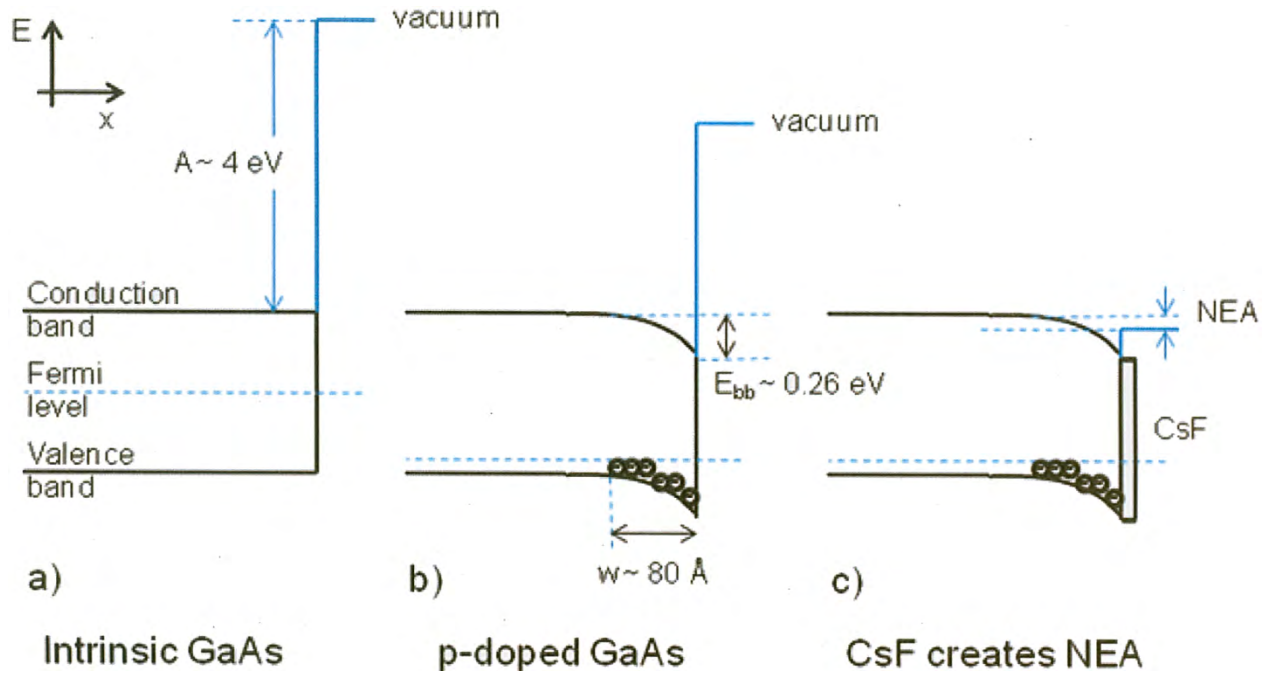

Figure 8.3. Energy level diagram of GaAs at the vacuum interface. (a) Undoped GaAs, (b) p-doped GaAs, and (c) with Cs and oxidant applied to the surface. *A* is the electron affinity; E_{bb}, is the energy offset associated with band bending region

While this sounds relatively simple, obtaining the expected amount of photoemission in practice can be difficult because the GaAs surface must be extremely clean and free of contamination at the atomic scale. Unfortunately, several steps are needed to insert a GaAs photocathode into a DC high voltage photogun, opening up many opportunities to contaminate the wafer. Once the photocathode is installed within the photogun, it must remain clean, meaning the photogun must function properly while delivering beam; the static vacuum inside the photogun must be extremely low and remain low while delivering the beam. The following sections describe typical photoguns and the steps required to install the clean photocathodes.

8.3 DESCRIPTION OF TYPICAL POLARIZED PHOTOGUN

DC high voltage, GaAs-based polarized photoguns are categorized as vent/bake or load-lock photoinjectors. In general, the former are considered easier to build, but require frequent maintenance, whereas the latter offer more accelerator up-time, once reliable sample manipulation has been demonstrated. Each type is described briefly below.

8.3.1 Vent/Bake Photoguns

Vent/bake photoguns must be vented to atmospheric pressure each time the photocathode is replaced and then baked for an extended time to recover the necessary vacuum level (see below). A typical vent/bake photogun shown in Figure **8.4** was successfully used at the CEBAF/Jefferson Laboratory for over ten years [8.17] and is described below. All the features needed to activate the photocathode to NEA, bias the photocathode at high voltage and generate high quality beam in an UHV environment are housed in a common vacuum chamber.

The photocathode is attached to the end of a long stalk extending into the gun vacuum chamber through the bore of the large cylindrical insulator, which is typical of the variety described in Chapter 4. Before

activating the photocathode to NEA, the photocathode must be heated to ~500 ˚C to liberate loosely bound adsorbed gas. Higher temperatures can "boil off" some surface contamination (oxides, in particular), but not carbon. Temperatures > 630 ˚C must be avoided as this causes the GaAs to decompose due to preferential evaporation of arsenic. To heat the photocathode, the stalk is retracted ~50 mm to avoid heating other parts of the gun and a resistive heater is inserted into the atmospheric side of the stalk in close mechanical contact. After the heat treatment, the photocathode is left to cool to room temperature and moved back into position within the cathode electrode for activation and beam generation. The cathode electrode has a 25˚ focusing angle and the anode is ~6 cm away. This geometry optimizes transport for the CEBAF beam with a maximum field gradient of ~5 MV m^{-1} when the cathode electrode is biased at -100 kV. Note that the cathode/anode geometry of each photogun depends heavily on the accelerator beam's specifications (*e.g.*, bunch charge) and typically is determined by computer simulations (*i.e.*, field mapping and particle tracking).

Non-evaporable getter (NEG) modules surround the cathode/anode gap, providing thousands of liters per second pumping for hydrogen. A small diode ion pump (not shown) pumps inert gasses, such as helium and methane that the NEGs do not pump efficiently. The photocathode is activated to NEA using cesium and flourine (or oxygen) sources located downstream of the anode. During activation, the drive laser can be directed on to the photocathode, or it can be illuminated from the side with a white light source, directed by a metallic mirror inside the vacuum chamber. The two chemicals, Cs and NF_3, are applied to the photocathode and metered while monitoring photocurrent that varies in a "yo-yo" manner (described below), although other groups follow different, but acceptable protocols. The chemical application is terminated once photocurrent ceases to increase appreciably, typically after ten yo-yos, with the net result corresponding to approximately one monolayer of chemical deposition. Cesium orginates from an alkali-metal dispenser from SAES Getters and is controlled by applying electrical current through a vacuum feedthough. The NH_3 is applied using a vacuum leak valve.

As mentioned above, the entire gun structure must be baked each time the photocathode is replaced. Bakeout temperature typically is ~250 ˚C and its duration is ~30 hr, although it can last longer if there is significant water vapor inside the vacuum chamber. High temperature bakeouts necessitate some precautions. For example, bare copper gaskets will oxidize during a bakeout. This is problematic because the oxide layer can "flake off" when flanges are disassembled, sometimes leading to a flange leak during a subsequent bakeout. To prevent this from happening, copper gaskets should be nickle-flashed and silver-plated to prevent oxidation. Silver-plated bolts are also recommended for the same reason. This ensures that nuts and bolts turn freely post-bakeout when the gun is disassembled. The NEG pumps can be electrically activated or passively activated to about 60% of their rated pump speed during the bakeout.

Besides the burden of vacuum-chamber bakeouts, which take days to complete, the most significant drawback of the vent/bake photogun design is the inadvertent application of cesium on the cathode electrode, which eventually leads to catastrophic field emission necessitating cathode electrode cleaning or replacement. The design in Figure **8.4** provides about seven full photocathode-activations before succumbing to field emission. Other gun designs at other laboratories fared better or worse; in hindsight, the results likely depended on the size of the anode hole and location of the cesium dispenser relative to the anode, which define the solid angle of cesium deposition at the photocathode and cathode electrode. Gun designs with small solid angle faired better than those that introduced more cesium on the cathode electrode.

8.3.2 Load-Lock Photoguns

Load-lock photoguns are comprised of multiple vacuum chambers separated by valves, with the vacuum improving from one chamber to the next, with the best vacuum obtained inside the gun's high voltage chamber. Reiterating, new photocathode samples can be installed without lengthy vacuum bake-outs of the entire gun; comprising one of the major benefits of the load-lock design. Another benefit is that cesium is not applied inadvertently to the cathode electrode since activation takes place inside another chamber. In this way, the cathode electrode remains pristine and it exhibits no field emission when biased at high voltage. Historically, most researchers have moved to a load-lock design to eliminate field emission.

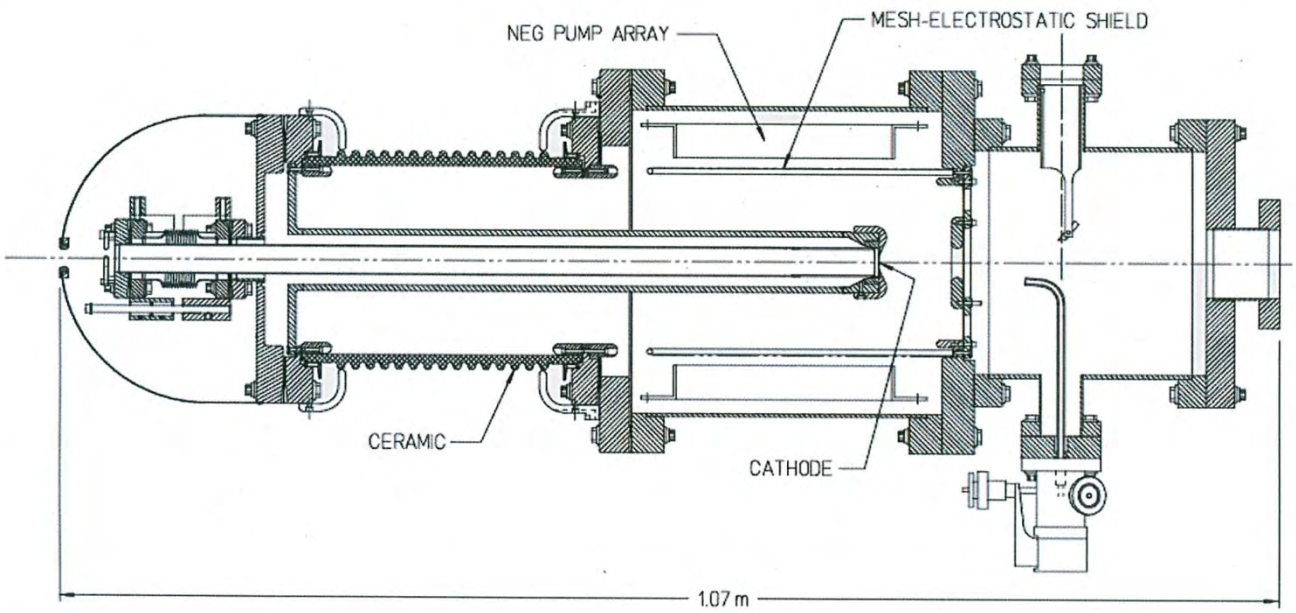

Figure 8.4. The CEBAF/Jefferson Lab vent/bake 100 kV DC high voltage, spin polarized GaAs photogun. It rests in the horizontal plane with the drive laser light introduced through a vacuum window to the right (not shown). [Adapted from [8.37], with permission from Elsevier]

The CEBAF/Jefferson Laboratory's load-lock gun is shown in Figure **8.5** [8.38]. It consists of four vacuum chambers: The high voltage chamber, the photocathode preparation chamber, a "suitcase" chamber used for replacing photocathode samples and an intermediary chamber that must be evacuated and baked each time the suitcase is attached. The suitcase normally is detached from the photogun and stored elsewhere. This approach helps to reduce the overall footprint of the photogun when in operation. Numerous alternative designs are used at laboratories worldwide [8.12], [8.13], [8.15], [8.16], [8.39], [8.40]. The ability to store multiple photocathode samples, reliable sample transport from one chamber to the next without dropping, and rapid heating and cooling of samples for fast turn-around at activation are some of the desirable features incorporated into most load-lock designs.

The high voltage chamber is similar to that of the vent/bake photogun described in Section 8.3.1, but lacks the components associated with photocathode activation. The NEG pump modules surround the cathode/anode gap and a small ion pump is used to pump inert gases.

Key features of the preparation chamber include storage for up to four pucks (each puck supports one photocathode), a mask for selective activation of a portion of the photocathode surface, puck heating to at least 600 ˚C, and good vacuum obtained using NEG and ion pumps. Photocathode activation takes place inside the preparation chamber using cesium and NF_3 similar to that described for the vent/bake photogun.

The preparation chamber has four magnetically coupled sample manipulators: one long manipulator with translation- and rotation-capability for moving pucks into or out of the gun's high voltage chamber cathode electrode; one short manipulator with translation- and rotation-capability for moving pucks from/on to the heater assembly and for transferring them to/from the long manipulator; and, two short manipulators with translation capability that hold pucks with additional photocathode samples.

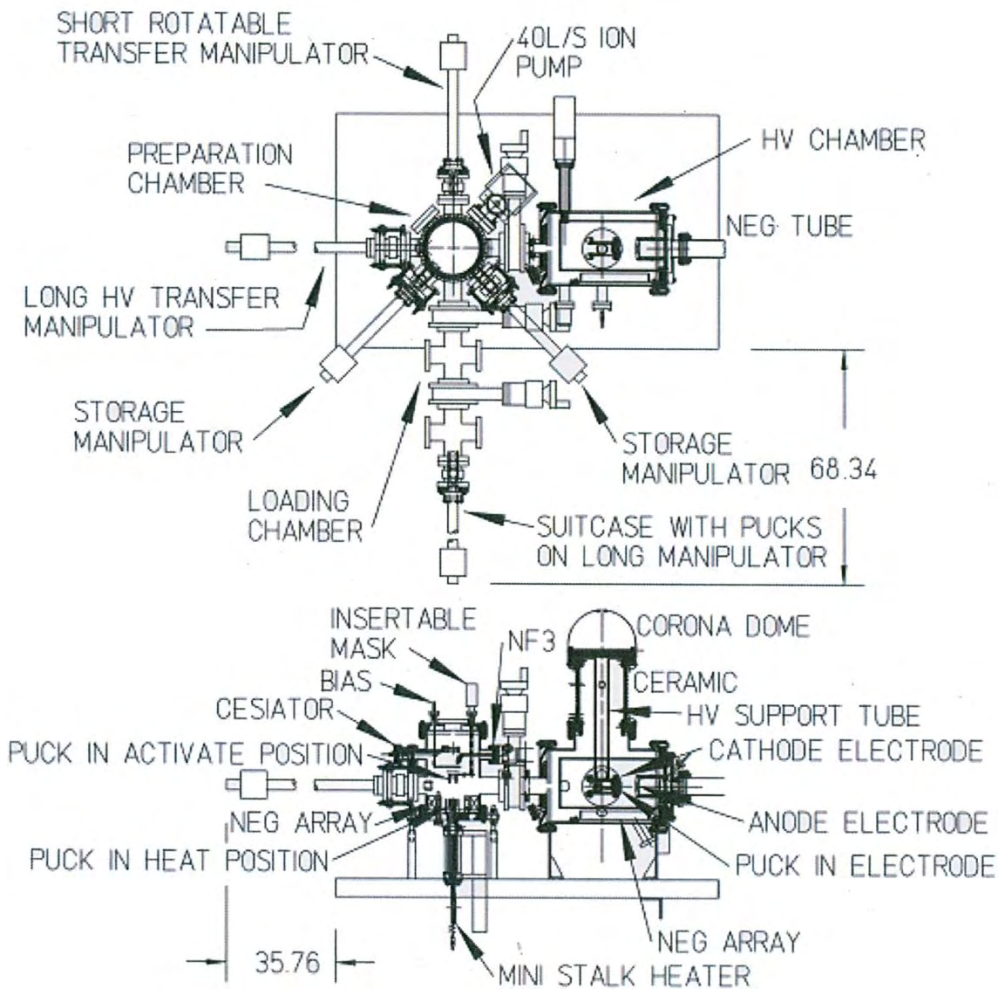

Figure 8.5. (Top) The plan view shows the complete gun assembly with four vacuum chambers: Gun High Voltage Chamber (large bore ceramic insulator design), Preparation Chamber, Intermediary Chamber and "Suitcase". (Bottom) The side view shows some of the components inside the preparation chamber including a heater that also serves to move the puck toward a mask used to selectively activate only the center portion of the photocathode. [Reprinted figure with permission from [8.38]. Copyright 2011 by the American Physical Society]

Care must be taken during the initial commissioning bake of the preparation chamber; the magnetic manipulators can develop excessive friction that limits functionality when heated above ~200 ˚C. Each magnetic manipulator is attached to a bellows assembly with adjustment screws for proper alignment to the electrode, heater and for other manipulators. Pumping inside the preparation chamber is provided by 40 L s^{-1} ion pump and 1.5 WP-1250 NEG modules from SAES Getters with support rods removed and coiled into the bottom of the vacuum chamber. Pressure inside the preparation chamber is ~1×10^{-8} Pa, which is adequate for preparing a photocathode with high QE; however, improved vacuum would provide a longer dark lifetime, *i.e.*, the QE lifetime of the photocathode when it is not biased at high voltage or illuminated with laser light.

8.4 OPERATION OF A DC HIGH VOLTAGE, SPIN-POLARIZED GaAs PHOTOGUN

8.4.1 Ion Bombardment

The photocathode lifetime of modern DC high voltage GaAs photoguns is limited primarily by ion bombardment, or ion back-bombardment [8.41]. This is the mechanism wherein residual gas is ionized by the extracted electron beam and transported backward to the photocathode, where the ions adversely affect the photocathode's QE. Exactly how the ions degrade QE is the subject of much speculation. While it was determined that ions with sufficient kinetic energy penetrate the photocathode's surface [8.42], it is not known what they do to the photocathode. They might damage the GaAs crystal structure, act as trapped interstitial defects that reduce the electron diffusion length, or act as unwanted dopant species, adversely altering the photocathode's energy band structure. Impinging ions may also sputter away the chemicals used to reduce the work function at the surface of the photocathode. Predicting which ions are the most problematic (gas species and energy) awaits a detailed modeling study that considers many parameters. The study should include relevant ion species with appropriate ionization cross sections, accurate trajectories of both ions and electrons, sputtering yield of alkali (cesium) and oxidant (fluorine) used to create the NEA condition at the photocathode surface required for photoemission and the stopping depths of ions within the photocathode. Parameters such as optical absorption length, electron-diffusion length and active layer thickness are likely to be important factors as well.

The ions produced by the electron beam arrive at the photocathode in a manner determined by the electrostatic field of the cathode/anode structure. When the drive laser beam is positioned at the center of the photocathode, all of the ions are delivered to the same location. When it is moved radially outward, ions are produced at the location of the laser beam and along a "trench" connecting the point of origin to the electrostatic center of the photocathode. Furthermore, ions produced downstream from the anode can arrive at the photocathode and hit the electrostatic center. A typical "QE scan" of a GaAs photocathode is shown in Figure **8.6**, illustrating QE reduction due to ion bombardment.

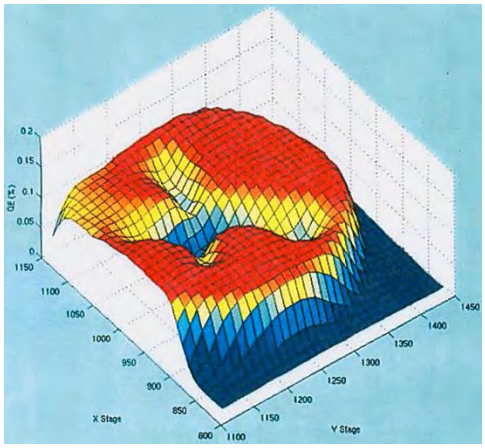

Figure 8.6. False-color QE map across the surface of a photocathode that has been damaged by ions. The colors denote the QE value at each photocathode location. The electron beam was extracted from three different radial locations. Note QE "trenches" that terminate at a common "electrostatic center". [Adapted with permission from [8.43]. Copyright 2007, American Institute of Physics]

The best strategy for minimizing QE decay associated with ion back-bombardment is to operate the photogun under an excellent vacuum. This includes static vacuum (no beam) and dynamic vacuum (while delivering the beam). A small cathode/anode gap is desirable to limit the number of ions created. However,

small gaps produce a large gradient which in turn enhance the field emission from the cathode electrode, which can significantly degrade the gun's performance *via* chemical poisoning of the photocathode surface and enhanced ion bombardment. A recent study [8.38] showed that the best operating lifetime can be obtained by operating with a laser beam positioned away from the electrostatic center and with an active area that minimizes the creation of "halo" beam that might not be efficiently transported away from the photogun.

8.4.2 Vacuum

As discussed, the longest photocathode lifetime is attained by minimizing ion bombardment which recommends operating the photogun in an exceptionally good vacuum. Equ. 10.2 provides remarkably useful insight toward appreciating the vacuum aspects of the photogun:

$$P_{ult} = \frac{(Gas\ Load)}{(Pump\ Speed)} \tag{8.2}$$

where P_{ult} is the ultimate pressure inside the gun. Obviously, it is beneficial to make the gas load inside the photogun small and the pump speed large.

To ensure a small gas load inside the photogun, several steps must be taken. First, proper UHV techniques must be practiced [8.44]. This includes constructing the photogun free of contamination. Manufactured parts typically are fabricated without oil or silicone lubricants and all components are cleaned in an ultrasonic bath of alkaline cleaner followed by acetone and hot de-ionized water. It also is very important to ensure that there are no virtual leaks inside the gun (*i.e.*, small spaces with trapped gas). For this reason, internal components are assembled with vented, silver-plated, stainless-steel screws.

After the photogun is constructed, it must be evacuated and baked to remove water vapor; typically, the gun is baked at 250 ˚C for 30 hr or longer. To assist this process, all CEBAF photoguns are built on tables with an insulating top large enough to accommodate oven panels that completely surround the gun. Heated air is directed into the enclosure using a 4 kW commercial heater system. The use of flowing hot air assures that the gun structure is heated uniformly without developing significant temperature differentials. As mentioned previously, nickel-flashed and silver-plated gaskets are recommended to avoid oxidation that can lead to flange leaks. The silver-plated, high-strength, stainless-steel bolts and stainless-steel nuts are easily disassembled post-bake. Belleville washers are used on flanges larger than 70 mm to assure reliable sealing during the expansion and contraction cycles of high temperature bakeouts.

When constructed properly, the gas load within the baked photogun originates from hydrogen out-gassing from the walls and internal components of the photogun. The typical out-gassing rate of 304 stainless steel is 1×10^{-10} Pa L s^{-1} cm^{-2}; with vacuum pumping from the NEGs and ion pump described below, it is not difficult to obtain pressure in the low 10^{-9} Pa range. Hotter bakeouts [8.45] provide lower out-gassing rates and proportionally lower pressure. High current applications benefit from extra effort to reduce the out-gassing rate of photogun components.

Ideally, when the valve to the beamline is opened, the gun vacuum should not degrade appreciably. This means that the beamline must be baked, and if space allows it is a good idea to incorporate a differential pump station near the gun to isolate the gun vacuum from the rest of the accelerator.
All modern DC high voltage, spin-polarized GaAs photoguns rely on NEG pumps and a small diode ion pump for removing inert gasses like He and methane which are not pumped by NEGs. NEG pumps provide

thousands of liters per second pump speed for hydrogen gas, the dominant gas species inside a UHV chamber. NEG pumps are commercial items purchased from SAES Getters, and the pumps that rely on ST707 material can be activated at relatively low temperature (~400 ˚C). Typically, a photogun design incorporates many NEG modules connected in series and electrically isolated inside the gun. The pumps are activated (*i.e.*, heated) by passing current through them.

8.5 PHOTOCATHODE PREPARATION

As described, several steps must be taken to insert a GaAs photocathode into a DC high voltage photogun, so there are many opportunities to contaminate the wafer. These steps include:

1. Cutting a photocathode sample from a large wafer supplied by the vendor.
2. Anodizing the edge of the photocathode to eliminate unwanted photoemission from region not supported by a proper electrostatic field. This step can be eliminated if a mask is used at activation.
3. Mounting the photocathode sample to a support structure that eventually will be positioned within the cathode electrode.
4. Baking the photocathode and support structure to achieve the required vacuum level.
5. Heating the photocathode to ~500 ˚C to liberate loosely bound gas before activation to NEA.

The exact details of these steps vary somewhat depending on the specific design of the photogun; for example, whether it is vented and baked each time the photocathode is replaced, or installed *via* a load-lock vacuum apparatus wherein the photocathode is mounted on to a small support structure and moved between different vacuum chambers. The text below describes features common to both gun designs and highlights some of the relevant differences.

8.5.1 Cutting GaAs to the Appropriate Shape and Size

GaAs material typically is sold in large circular discs which are flat at one edge to indicate the direction of the cleave plane. The disc is usually ~600 μm thick and 50-75 mm in diameter. This large wafer must be cut into smaller samples for installing into photoguns. Originally at CEBAF/Jefferson Laboratory, samples were cut from large wafers using a circular-shaped cutting jig and diamond-paste slurry. The large wafer was sandwiched between glass slides using an acetone-soluble adhesive to protect the surface of the photocathode during cutting. This process was time consuming and invariably introduced a significant amount of contamination on the surface of the photocathode which needed to be removed using strong acids/bases or *via* hydrogen cleaning. This cutting technique was replaced with a far simpler cleaving technique. Now, a diamond-tipped scribe is used to cleave square samples from large wafers. Aside from the diamond-tip scribe, nothing touches the surface of the photocathode material during cleaving, and as a result, the photocathode surface is not contaminated.

8.5.2 Anodizing the Edge of the Photocathode to Limit QE

It is very important to eliminate unwanted and inadvertent photoemission from the edge of the photocathode – photoemission that is not properly tranported away from the gun results in the halo effect. Photoemission from the edge of the photocathode follows extreme trajectories, striking the vacuum chamber wall downstream of the gun and even hitting the anode plate. This degrades the vacuum in the gun hastening the photocathode's QE decay. Anodizing the edge of the photocathode in an electrolytic bath is one way to eliminate photoemission from the edge.

A fixture was devised that holds the photocathode, sandwiched between two Viton O-rings. One O-ring prevents electrolytic fluid from contacting the center portion of the front face, while the other merely provides a surface to securely and carefully hold the wafer without breaking it. Clean distilled water with a

few drops of phosphoric acid provides an adequate pH level for anodizing. In just a few seconds, a thick oxide layer forms on the photocathode's edge that assures no measureable photoemission; the oxide layer will not evaporate during bakeouts or photocathode heating.

For load-lock guns, an activation mask can be used to selectively activate only the center portion of the photocathode, eliminating the anodizing step and saving a considerable amount of time.

8.5.3 Mounting the Photocathode to Support Structure

Next, the small photocathode samples are indium-soldered to a molybdenum support (*i.e.*, the stalk or puck) at ~200 ˚C inside a nitrogen-filled glove box. Molydenum is a good material for supporting the photocathode sample because of its small coefficient of thermal expansion and UHV compatibility. Indium provides mechanical stability and good heat conduction (the GaAs must be heated to ~500 ˚C to remove the weakly bound gas before activation). A tantalum retaining ring then is placed over the GaAs wafer and crimped in place, thereby ensuring that the GaAs wafer is never dislodged inadvertently from the support structure.

8.5.4 Installing the Photocathode into the Photogun Vacuum Chamber: Bakeout, Heating and Activating the Photocathode

The GaAs wafer, mounted to its support structure and loaded into the gun vacuum chamber using a nitrogen-filled glove bag. The gun is pumped down with a clean, oil-free, rough pump. Once the pressure drops sufficiently low to energize the gun ion pump, the valve to the rough pump is closed. The entire photogun chamber is then baked, as described above. It is important to ensure that the GaAs photocathode remains clean during the bakeout. To do so, one must minimize the time spent venting and pumping down the vacuum chamber and vent the vacuum chamber with clean, dry nitrogen gas pressurized to assure minimal back-diffusion during the photocathode exchange. With these precautions, pump-down from atmospheric pressure is rapid, *i.e.* the pressure typically falls below 10^{-6} Pa within 20 min after starting pumping. It is good practice to not allow the pressure to rise above ~1×10^{-5} Pa during bakeout.

Once the bakeout is complete, the photocathode can be activated to NEA. First, the photocathode is heated to ~500 ˚C to liberate loosely bound adsorbed gas from its surface: two hours is sufficient at this temperature. Once the photocathode has cooled to ~30 ˚C, activation begins with the successive application first of cesium, then of NF_3 (or oxygen). During activation, the cathode is biased at ~-200 V and illuminated with light. On initial exposure to cesium, the photoemission current reaches a maximum and then decreases. A typical approach (called the "yo-yo" process) allows the photocurrent to decrease to about half of its maximum value before stopping the cesium exposure. On subsequent exposure to NF_3, the photocurrent rapidly increases to a new maximum, saturates and then slowly decreases. Further exposure to cesium quickly produces a rapid decrease in the photocurrent. Again, we allow the photocurrent to fall to about half and follow it with another exposure to nitrogen trifluoride. Typically, ten cycles of Cs/NF_3 are required to reach the final quantum efficiency.

To assess how well the photocathode was installed, it is customary to evaluate the QE. It can be written in terms of easily measured quanitities such that

$$\mathrm{QE} = \frac{(\#\ photoemitted\ electrons)}{(\#\ incident\ photons)} = 124\,\frac{I}{\lambda P_{inc}} \tag{8.3}$$

where I is the photocurrent in microamperes, λ is the laser wavelength in nanometers and P_{inc} is incident laser power in milliwatts. Table **8.1** lists typical QE values from clean photocathode material illuminated with near-band gap light appropriate for high polarization.

Material	Wavelength [nm]	QE [%]	Polarization [%]
"Bulk" GaAs	780	~10	~35
Strained layer GaAs/GaAsP	850	~0.1	~75
Strained-Superlattice GaAs/GaAsP	780	~1	~85

Table 8.1. Typical QE and polarization for common GaAs photocathodes.

8.5.5 Hydrogen Cleaning

Edge-anodizing is a step that most often introduces contaminants onto the photocathode surface. Baking the photocathode within the gun at high pressure, *e.g.* due to excessive amounts of water in the gun, is another opportunity for contamination. There are many recipes for cleaning semiconductor surfaces with wet chemical solutions of strong acids and/or bases; however, experience at Jefferson Lab with wet chemical cleaning techniques was mixed. Moreover, these techniques remove the surface layer significantly, a situation that is unacceptable when using high polarization photocathodes. Therefore, we adopted an alternative cleaning procedure using atomic hydrogen, exposure to which has shown to remove surface contaminants such as carbon and oxygen from a wide variety of semiconductors [8.46]–[8.50]. Furthermore, as noted in [8.51], hydrogen atoms passivate the dangling bonds at the GaAs surface, leaving a relatively inert surface, ideal for bakeouts.

RF-dissociators and thermal crackers are common sources of atomic hydrogen. At the CEBAF/Jefferson Lab, the RF-dissociator approach is used, although there is some concern that this method roughens the photocathode surface. Molecular hydrogen from a small research-grade bottle is fed through a Pyrex cylinder at about 2 mPa (Figure **8.7**). A 12-turn coil surrounds the Pyrex tube and a plasma is formed when the applied RF (~50 W) is resonant with the circuit. Atomic hydrogen exits the chamber through a ~1 mm diameter hole and is guided *via* an aluminum tube (aluminum has a low recombination rate) to the photocathode sample about 15 cm away. The photocathode sample is held at 300 ˚C during hydrogen cleaning [8.48], [8.49]. A small turbo-molecular pump and an ion pump maintain pressure near the photocathode sample at ~10^{-3} Pa during cleaning to provide a long mean-free path for the atoms and ensure the atoms hit the photocathode before recombining into molecules. Monte Carlo simulations predict that ~2.5% of the total atom flux reaches the photocathode. Under these conditions, the estimated atom flux at the cathode is ~10^{17} atoms cm^{-2} sec^{-1}, assuming 50% dissociation [8.51].

After hydrogen cleaning, the stalk and photocathode are installed within the photogun using a nitrogen-filled glove bag. Hydrogen cleaning has an added benefit of yielding a chemically inert surface that helps to keep the photocathode clean during the bake-out of the photogun. Load-lock gun systems also employ hydrogen cleaning for in-*situ* cleaning.

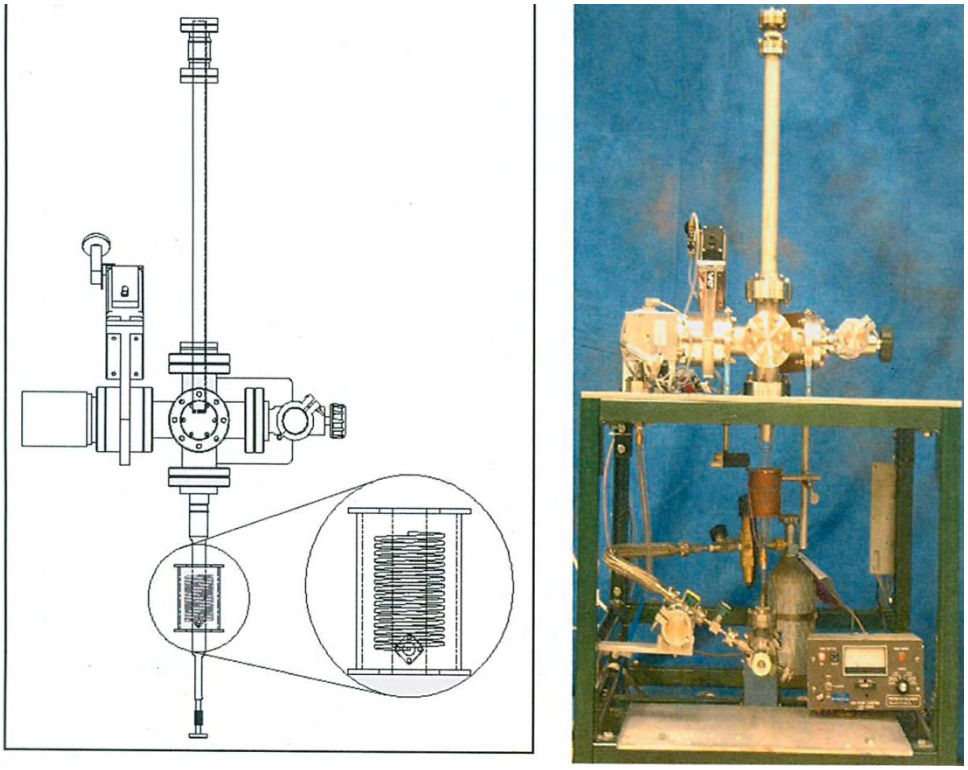

Figure 8.7. The RF-dissociator, atomic hydrogen cleaning apparatus using at CEBAF/Jefferson Laboratory. [Reprinted/Adapted figures with permission from [8.31]. Copyright 2005 by the American Physical Society]

8.6 DRIVE LASERS FOR A POLARIZED BEAM

A DC laser light source can be used to make an electron beam at an accelerator, but something must be done to create the appropriate RF time structure necessary for acceleration. Typically, this means using RF bunching cavities or RF choppers; however, bunching introduces energy spread and chopping is very inefficient, with a significant amount of the beam simply thrown away. At CEBAF, these ill effects were overcome by implementing synchronous photoinjection, a process whereby RF structure is created directly at the photocathode using an RF-pulsed drive laser. In the early 1990s, synchronous photoinjection with a GaAs photocathode had not been demonstrated. In fact, some thought it would not be possible, suggesting that GaAs would not respond quickly enough to the short-pulse light [8.36]. However, this concern proved unwarranted and synchronous photoinjection with GaAs now is widely used at many accelerators [8.53], [8.54], [8.55].

Mode-locked lasers often are used for synchronous photoinjection (see Chapter 9), but gain switching [8.56] is the preferred pulse-forming technique employed at CEBAF. Gain switching is a purely electrical technique that relies on diode lasers. By simply applying a ~1 W RF sine wave to the diode laser, ~30-50 ps optical pulses can be obtained at repetition rates between 100-3 000 MHz. This optical pulse-train can be easily locked to the accelerator RF frequency and a feedback loop is not required to maintain a fixed laser cavity length, as required when using mode-locked lasers. A gain-switched diode, however, can only produce a few milliwatts average power, and so, for most accelerators, a laser amplifier is required to boost power to an acceptable level. Diode lasers are available readily at wavelengths between 780 and 850 nm and single-pass traveling wave-tapered stripe diode amplifiers can generate ~100 mW. For higher power applications, fiber-based laser components from the telecom industry now are the best choice. Light at 1560 nm from a fiber-coupled, gain-switched seed laser can be sent to a fiber amplifier and then frequency

doubled to produce Watts of useful light at 780 nm [8.57] (Figure **8.8**). Similar fiber-based systems are used to generate high power at 532 nm [8.55].

Standard optical components are used to deliver the laser light to the photocathode. The main distinction between polarized photoelectron guns and non-polarized photoguns is that the drive laser's light must be circularly polarized and have the appropriate wavelength. Thin mica wave-plates can generate circularly polarized light and the sign of the polarization can be flipped by moving wave-plates in/out of the laser beam's path. Faster spin-flipping can be achieved by using an electro-optic modulator called a Pockels cell, where two spin states are obtained by reversing the polarity of voltage applied to the Pockels cell. As an example, for typical experiments at CEBAF, the polarization direction flips at 30 Hz. Recently a technique was developed to flip polarization at rates up to 1000 Hz [8.58].

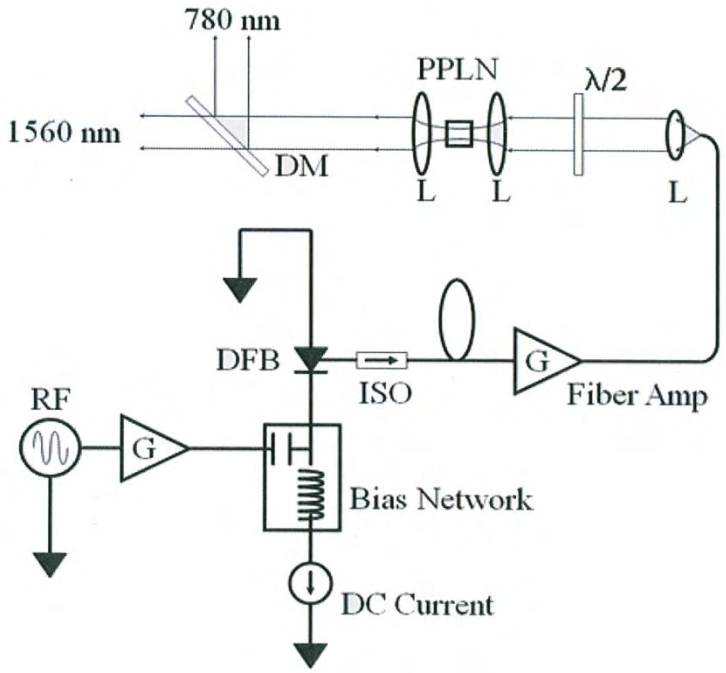

Figure 8.8. Schematic of the fiber-based laser system with gain-switched diode master oscillator. The following list consists of the acronyms used in the figure: DFB, distributed feedback Bragg reflector diode laser; ISO, fiber isolator; G, amplifier gain; L, lens; PPLN, periodically poled lithium niobate frequency doubling crystal; and DM, dichroic mirror. [Reprinted figure with permission from [8.57]. Copyright 2006 by the American Physical Society]

8.7 SPIN MANIPULATION

Polarized-beam experiments require a specific orientation of the direction of electron spin at the target, typically parallel to that of beam motion. Electrons leave the photocathode with their spin direction pointing parallel/antiparallel to the direction of beam motion, depending on the helicity of the laser's circular polarization (right or left circular) created by the Pockels cell. However, the spin direction precesses in the horizontal plane as the beam passes through the arcs and transport lines to the halls; this net spin precession must be "cancelled out" by orienting the spin direction at the injector by the opposite amount using a spin manipulator. At CEBAF, a Wien filter is used for spin manipulation [8.17]. It is a device with static electric- and magnetic-fields perpendicular to each other and to the velocity of charged particles passing through it (Figure **8.9**). Unit charged particles with a velocity of $\beta c = E\,B^{-1}$ remain undeflected in passing through the Wien filter, while the spin is rotated in the plane of the electric field. A window-frame dipole magnet provided the magnetic field. The magnet was terminated at each end with a nickel plate with a 20 mm

diameter beam aperture. We carefully mapped the magnetic field of the full magnet, assembled on the Wien filter vacuum chamber, with a precision Hall probe. We then calculated the profile of the electric field plates, using the code POISSON [8.59], to produce an electric field whose profile closely matches that of the magnetic field. The Wien filter can rotate the spin by ±110˚ at 100 keV. The calibration and performance of this Wien filter is described in Grames *et al.* [8.60].

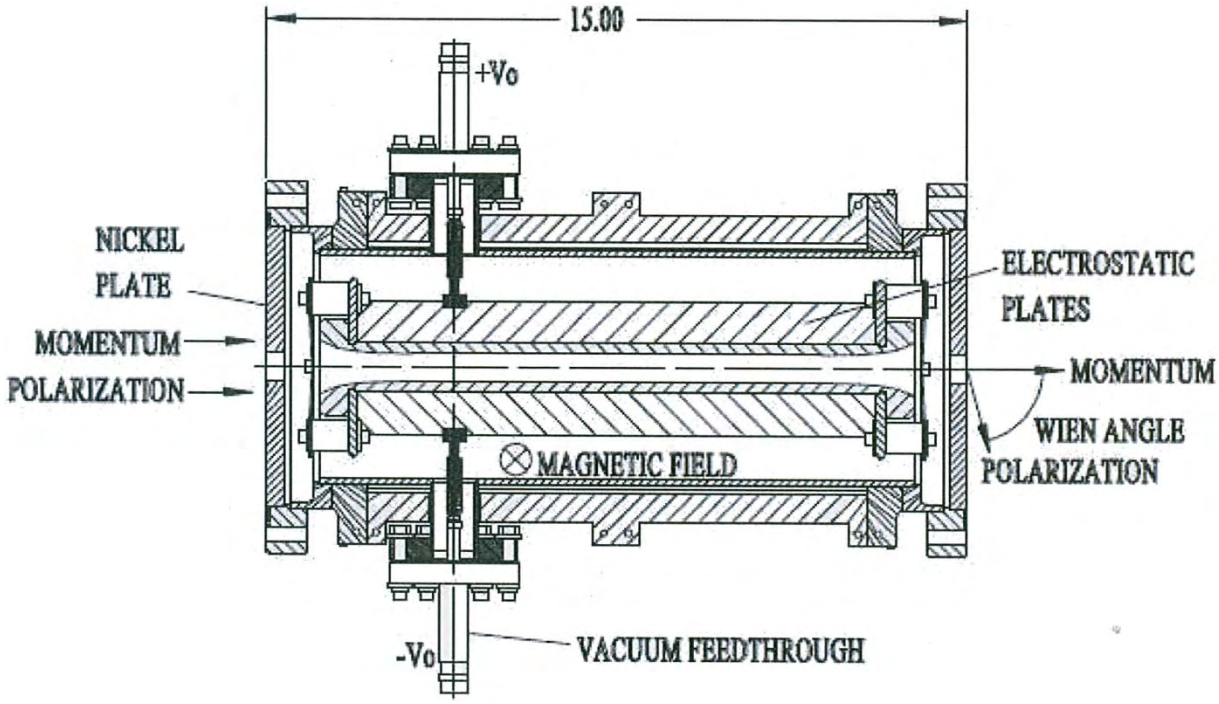

Figure 8.9. The Wien filter spin manipulator used with CEBAF's second and third polarized electron sources. The magnet is not shown in this cutaway view. [[8.61]; Available under Creative Common Attribution 3.0 License (www.creativecommons.org/licenses/by/3.0/us/) at www.JACoW.org.]

8.8 POLARIMETRY

After making a spin-polarized electron beam, the magnitude of the polarization must be measured. Typically, this is done using Mott polarimetry [8.62] that can accommodate electron beam energies between a few kiloelectron volts and a few megaelectron volts. A Mott polarimeter relies on the scattering asymmetry observed when spin-polarized electrons – with the spin vector oriented perpendicular to the scattering plane – strike the nuclei of an unpolarized target. To make a polarization measurement, a scattering asymmetry is measured using detectors that count the number of electrons that scatter to the right/left (or up/down) as the direction of the electron spin is flipped by changing the helicity of the circular polarization of the photogun drive laser's light (*via* the laser-table electro-optic Pockels cell, described above). The measured scattering asymmetry, A, is related to beam polarization, P, and the effective Sherman function, S_{eff}, as given below:

$$A = \frac{(\mathrm{N}\rightarrow - \mathrm{N}\leftarrow)}{(\mathrm{N}\rightarrow + \mathrm{N}\leftarrow)} = S_{eff} \tag{8.4}$$

The Sherman function, or analyzing power, is a term associated with the physics of the scattering process. The *effective* Sherman function describes the same process, but modified to account for real life experimental conditions, *e.g.* multiple scattering and detector acceptance. The most desirable characteristic

of any polarimeter is a large and well known effective Sherman function; however, in practice, this value must be determined by computer simulation and/or detailed experimental measurements, *e.g.*, extrapolating target thickness, or retarding field scans.

The subject of Mott polarimetry is broad enough to be the focus of another book. Suffice to say, there are different types of Mott polarimeters that can be categorized loosely according to their electron beam energies: Low voltage retarding field Mott polarimeters, conventional gun-voltage Mott polarimeters and accelerator based MeV Mott polarimeters. Of these, the last are the most accurate (~1%) because experimental measurements can be predicted very accurately using a model that successfully accounts for multiple scatterings within the target foil [8.63]. For conventional Mott polarimetry at gun voltage (~100 kV), the effective Sherman function is determined empirically by performing a foil thickness extrapolation to deduce the asymmetry associated with single-scattering events [8.20]. For retarding field Mott polarimetry [8.64], a low voltage beam (~-200 V) is accelerated toward a thick target biased at ~20 kV. Electrons with a broad energy spectrum arrive at the detectors, but the single scattering events can be discerned by biasing the detectors at the photocathode voltage.

8.9 FUTURE R&D

Although a number of laboratories that provided spin-polarized electron beams have closed (NIKHEF, MIT-Bates and SLAC), there is still great interest within the scientific physics community to conduct experiments with polarized electron beams. Future R&D will focus on enhancing beam polarization and providing significantly higher current (milliamperes). These goals will spur exciting developments in the sub-fields of vacuum, drive lasers, high voltage and elimination of field emission. It seems reasonable to anticipate having a spin polarized beam from an RF gun, which is appealing for high-bunch charge accelerator applications that demand a small beam emittance.

8.10 CONFLICT OF INTEREST AND ACKNOWLEDGEMENT

We confirm that this article content has no conflicts of interest and would like to acknowledge the support of U.S. DOE Contract No. DE-AC05-84ER40150.

References

[8.1] J. Kessler, *Polarized Electrons*, Berlin: Springer-Verlag, 1985.

[8.2] E. Leader, *Spin in Particle Physics*, Cambridge: Cambridge University Press, 2001.

[8.3] M. J. Alguard, J. E. Clendenin, R. D. Ehrlich *et al.*, "A source of highly polarized electrons at the Stanford linear accelerator center," *Nucl. Instrum. Meth.*, vol. 163, pp. 29-59, July 1979.

[8.4] W. von Drachenfels, U. T. Koch, Th. M. Müller *et al.*, "A pulsed source for polorized electrons with high repetition rate," *Nucl. Instrum. Meth.*, vol. 140, pp. 47-55, January 1977.

[8.5] M. J. Alguard, J. E. Clendenin, P. S. Cooper *et al.*, "Depolorization effects in pulsed photoionization of state-selected lithium," *Phys. Rev. A*, vol. 16, pp. 209-212, July 1977.

[8.6] L. A. Hodge, F. B. Dunning and G. K. Walters, "Intense source of spin-polarized electrons," *Rev. Sci. Instrum.*, vol. 50, pp. 1-4, January 1979.

[8.7] P. F. Wainwright, M. J. Alguard, G. Baum *et al.*, "Applications of a DC Fano effect polarized election source to low-energy electron-atom scattering," *Rev. Sci. Instrum.*, vol. 49, pp. 571-585, May 1978.

[8.8] D. T. Pierce, F. Meier and P. Zürcher, "Negative electron affinity GaAs: A new source of spin-polarized electrons," *Appl. Physics Lett.*, vol. 26, pp. 670-672, June 1975.

[8.9] C. K. Sinclair, E. L. Garwin, R. H. Miller *et al.*, "A high intensity polarized electron source for the Stanford linear accelerator," in *Proc.AIP Conf.*, vol. 35, 1976, pp. 424-431.

[8.10] C. Y. Prescott, W. B. Atwood *et al.*, "Parity non-conservation in inelastic electron scattering," *Physics Lett. B*, vol. 77, pp. 347-352, August 1978.

[8.11] K. Wada, M. Yamamoto, T. Nakanishi *et al.*, "200 keV polarized electron source at Nagoya University," in *Proc. 15th Int. Spin Physics Symp.*, 2003, 1063-1067.

[8.12] W. Hartmann, D. Conrath, W. Gasteyer *et al.*, "A source of polarized electrons based on photoemission of GaAsP," *Nucl. Instrum. Meth. A*, vol. 286, pp. 1-8, January 1990.

[8.13] K. Aulenbacher, Ch. Nachtigall, H. G. Andresen *et al.*, "The MAMI source of polarized electrons," *Nucl. Instrum. Meth. A*, vol. 391, pp. 498-506, June 1997.

[8.14] G. D. Cates, V. W. Hughes, R. Michaels *et al.*, "The Bates polarized electron source," *Nucl. Instrum. Meth. A*, vol. 278, pp. 293-317, June 1989.

[8.15] M. J. J. van den Putte, C. W. De Jager, S. G. Konstantinov *et al.*, "The polarized electron source at NIKHEF," in *Proc. AIP Conf.*, vol. 421, 1997, pp. 260-269.

[8.16] W. Hillert, M. Govin and B. Neff, "The 50 keV inverted source of polarized electrons at ELSA," in *Proc. AIP Conf.*, vol. 570, 2000, pp. 961-964.

[8.17] C. K. Sinclair, P. A. Adderley, B. M. Dunham *et al.*, "Development of a high average current polarized electron source with long cathode operational lifetime," *Phys. Rev. ST Accel. Beams*, vol. 10, pp. 023501-1–023501-21, February 2007.

[8.18] S. M. Sze, *Physics of Semiconductor Devices*, New York: John Wiley & Sons, 1981.

[8.19] J. S. Blakemore, "Semiconducting and other major properties of gallium arsenide," *J. Appl. Physics*, vol. 53, pp. R123-R181, October 1982.

[8.20] D. T. Pierce and F. Meier, "Photoemission of spin-polarized electrons from GaAs," *Phys. Rev. B*, vol. 13, pp. 5484-5500, June 1976.

[8.21] G. L. Bir, A. G. Aronov and G. E.Piku, "Spin relaxation of electrons due to scattering by holes," *Soviet Physics J. Experimental Theoretical Physics*, vol. 42, 705, October 1975.

[8.22] M. I. D'Yakonov and V. I. Perel, "Spin orientation of electrons associated with the interband absorption of light in semiconductors," *Soviet Physics J. Experimental Theoretical Physics*, vol. 33, pp. 1053-1059, November 1971.

[8.23] R. J. Elliott, "Theory of the effect of spin-orbit coupling on magnetic resonance in some semiconductors," *Phys. Rev.*, vol. 96, pp. 266-279, October 1954.

[8.24] Y. Yafet, *Solid State Physics*, vol. 14, New York: Academic Press, 1963, Chap. 1, pp. 1.

[8.25] M. Zolotorev, "Effects of radiation trapping on polarization of photoelectrons from semiconductors," in *Proc. Workshop Photocathodes Polarized Electron Sources Accelerator*, 1993, pp. 435-444.

[8.26] T. Maruyama, E. L. Garwin, R. Prepost *et al.*, "Observation of strain-enhanced electron-spin polarization in photoemission from InGaAs," *Phys. Rev. Lett.*, vol. 66, pp. 2376-2379, May 1991.

[8.27] T. Nakanishi, H. Aoyagi, H. Horinaka *et al.*, "Large enhancement of spin polarization observed by photoelectrons from a strained GaAs layer," *Physics Lett. A*, vol. 158, pp. 345-349, September 1991.

[8.28] T. Maruyama, E. L. Garwin, R. Prepost *et al.*, "Electron-spin polarization in photoemission from strained GaAs grown on $GaAs_{1-x}P_x$," *Phys. Rev. B*, vol. 46, pp. 4261-4264, August 1992.

[8.29] T. Nakanishi, S. Okumi, K. Togawa *et al.*, "Highly polarized electrons from superlattice photocathodes," in *Proc. AIP Conf.*, vol. 421, 1998, p. 300-310

[8.30] T. Maruyama, D.-A. Luh, A. Brachmann *et al.*, "Systematic study of polarized electron emission from GaAs/GaAsP superlattice photocathodes," *Appl. Phys. Lett.*, vol. 85, pp. 2640-2642, September 2004.

[8.31] M. Baylac, P. Adderley, J. Brittian *et al.*, "Effects of atomic hydrogen and deuterium exposure on high polarization GaAs photocathodes," *Phys. Rev. ST Accel. Beams*, vol. 8, pp. 123501-1–123501-11, December 2005.

[8.32] SPIRE Semiconductor, L.L.C., 25 Sagamore Park Drive, Hudson, NH 03051, http://www.spirecorp.com/spire-bandwidth-semiconductor/index.php.

[8.33] SVT Associates, Inc., 7620 Executive Drive, Eden Prairie, MN 55344, http://www.svta.com.

[8.34] Yu. A. Mamaev, L. G. Gerchikov, Yu. P. Yashin *et al.*, "Optimized photocathode for spin-polarized electron sources," *Appl. Phys. Lett*., vol. 93, pp. 81114-1–81114-3, August 2008.

[8.35] T. Nishitani, M. Tabuchi, Y. Takeda *et al.*, "Superlattice photocathode with high brightness and long NEA-surface lifetime," in *Proc. AIP Conf.*, vol. 1149, 2009, pp 1047-1051.

[8.36] W. E. Spicer and A. Herrera-Gómez, "Modern theory and applications of photocathodes," in *Int. 1993 Symp. Imaging Instrumuments*, 1993, pp. 18-33.

[8.37] M. L. Stutzman, P. Adderley, J. Brittian *et al.*, "Characterization of the CEBAF 100 kV dc GaAs photoelectron gun," *Nucl. Instrum. Meth. A*, vol. 574, pp. 213-220, May 2007.

[8.38] J. Grames, R. Suleiman, P. A. Adderley *et al.*, "Charge and fluence lifetime measurements of a DC high voltage GaAs photogun at high average current," *Phys. Rev. ST Accel. Beams*, vol. 14, pp. 043501-1–043501-12, April 2011.

[8.39] M. Breidenbach, M. Foss, J. Hodgson *et al.*, "An inverted-geometry, high voltage polarized electron gun with UHV load lock," *Nucl. Instrum. Meth. A*, vol. 350, pp. 1-7, October 1994.

[8.40] R. Alley, H. Aoyagi, J. Clendenin *et al.*, "The Stanford linear accelerator polarized electron source," *Nucl. Instrum. Meth. A*, vol. 365, pp. 1-27, November 1995.

[8.41] K. Aulenbacher, H. G. Andresen, T. Dombo *et al.*, "Operating experience with the MAMI polarized electron source," in *Proc. Workshop Photocathodes Polarized Electron Sources Accelerators*, 1994, pp. 1-12.

[8.42] M. L. Stutzman and J. Grames, "Superlattice photocathode damage analysis," in *Proc. AIP Conf.*, vol. 1149, 2008, pp. 1032-1037.

[8.43] J. Grames, P. Adderley, J. Brittian *et al.*, "A biased anode to suppress ion back-bombardment in a dc high voltage photoelectron gun," in *Proc. AIP Conf.*, vol. 980, 2007, pp. 110-117.

[8.44] P. A. Redhead, "Ultrahigh and Extreme High Vacuum," in *Foundations of Vacuum Science and Technology*, New York: Wiley, 1998, Chap. 11.

[8.45] C. D. Park, S. M. Chung, X. Liu *et al.*, "Reduction in hydrogen outgassing from stainless steels by a medium-temperature heat treatment," *J. Vac. Sci. Technology A*, vol. 26, pp. 1166-1171, August 2008.

[8.46] M. Yamada and Y. Ide, "Direct observation of species liberated from GaAs native oxides during atomic hydrogen cleaning," *Japanese J. Appl. Physics*, vol. 33, pp. L671-L674, March 1994.

[8.47] Y. Ide and M. Yamada, "Role of Ga_2O in the removal of GaAs surface oxides induced by atomic hydrogen," *J. Vac. Sci. Technology A*, vol. 12, pp. 1858-1863, July 1994.

[8.48] E. Petit, F. Houzay and J. M. Moison, "Interaction of atomic hydrogen with native oxides on GaAs (100)," *J. Vac. Sci. Technology A*, vol. 10, pp. 2172-2177, July 1992.

[8.49] E. Petit and F. Houzay, "Optimal surface cleaning GaAs (001) with atomic hydrogen," *J. Vac. Sci. Technology B*, vol. 12, pp. 547-550, March 1994.

[8.50] S. Sugata, A. Takamori, N. Takado *et al.*, "GaAs cleaning with a hydrogen radical beam gun in an ultrahigh-vacuum system," *J. Vac. Sci. Technology B*, vol. 6, pp. 1087-1091, July 1988.

[8.51] Y. Okada and J. S. Harris, "Basic analysis of atomic-scale growth mechanics for molecular beam epitaxy of GaAs using atomic hydrogen as a surfactant," *J. Vac. Sci. Technology B*, vol. 14, pp. 1725-1728, May 1996.

[8.52] M. Poelker, K. P. Coulter, R. J. Holt *et al.*, "Laser-driven source of spin polarized atomic hydrogen and deuterium," *Nucl. Instrum. Meth. A*, vol. 364, pp. 58-69, September 1995.

[8.53] K. Aulenbacher, H. Euteneuer, D. von Harrach *et al.*, "High capture efficiency for the polarized beam at MAMI by R.F.-synchronized photoemission," in *Proc. 6th European Particle Accelerator Conf.*, 1998, pp. 1388-1390.

[8.54] S. Benson, G. Biallas, C. Bohn *et al.*, "First lasing of the Jefferson Lab IR demo FEL," *Nucl. Instrum. Meth. A*, vol. 429, pp. 27-32, June 1999.

[8.55] D. Ouzounov, H. Li, B. Dunham and F. Wise, "Fiber-based drive laser systems for the Cornell ERL electron photoinjector," in *Proc. SPIE Conf.*, vol. 7581, 2010, pp. 75810N-1–75810N-11.

[8.56] M. Poelker, "High power gain-switched diode laser master oscillator and amplifier," *Appl. Physics Lett.*, vol. 67, pp. 2762-2764, August 1995.

[8.57] J. Hansknecht and M. Poelker, "Synchronous photoinjection using a frequency-doubled gain-switched fiber-coupled seed laser and ErYb-doped fiber amplifier," *Phys. Rev. ST Accel. Beams*, vol. 9, pp. 063501-1–063501-5, June 2006.

[8.58] J. Hansknecht, "Pockels cell switching method," [Online]. Available: http://www.jlab.org/accel/inj_group/laser2001/pockels_files/pockels_switch_notebook.htm [Accessed: January 31, 2012]

[8.59] K. Halbach, "Program for inversion of system analysis and its applications to the design of magnets," Lawrence Berkley Radiation Laboratory, Technical Report No. UCRL-17436, January 1967.

[8.60] J. M. Grames, C. K. Sinclair, J. Mitchell *et al.*, "Unique electron polarimeter analyzing power comparison and precision spin-based energy measurment," *Phys. Rev. ST Accel. Beams*, vol. 7, pp. 042802-1–042802-18, April 2004.

[8.61] J. Grames, P. Adderley, J. Benesch *et al.*, "Two wien filter spin flipper," in *Proc. 2011 Particle Accelerator Conf.*, 2011, pp. 862-864.

[8.62] T. J. Gay and F.B. Dunning, "Mott electron polarimetry," *Rev. Sci. Instrum.*, vol. 63, pp. 1635-1651, October 1992.

[8.63] M. Steigerwald, "MeV Mott polarimetry at Jefferson Lab," in *Proc. AIP Conf.*, vol. 570, 2001, pp. 935-942.

[8.64] J. L. McCarter, M. L. Stutzman, K. W. Trantham *et al.*, "A low-voltage retarding-field Mott polarimeter for photocathode characterization," *Nucl. Instrum. Meth. A*, vol. 618, pp. 30-36, June 2010.